Macromolecules

ARTICLE

pubs.acs.org/Macromolecules

Mixed-Salt Effects on the Ionic Conductivity of Lithium-Doped PEO-Containing Block Copolymers

Wen-Shiue Young, Julie N. L. Albert, A. Benjamin Schantz, and Thomas H. Epps, III*

Department of Chemical Engineering, University of Delaware, Newark, Delaware 19716, United States

ABSTRACT: We demonstrate a simple, yet effective, mixed-salt method to increase the room temperature ionic conductivity of lithium-doped block copolymer electrolyte membranes by suppressing the crystalline phases in the conducting block. We examined a mixed-salt system of $LiClO_4$ and $LiN(SO_2CF_3)_2$ (LiTFSI) doped into a lamellae-forming poly(styrene-*b*-ethylene oxide) (PS−PEO) diblock copolymer. The domain spacings, morphologies, thermal behavior, and crystalline phases of salt-doped PS−PEO samples were characterized, and the ionic conductivities of block copolymer electrolytes were obtained through ac impedance measurements. Comparing the ionic conductivity profiles of salt-doped PS−PEO samples at different mixed-salt ratios and total salt concentrations, we found that the ionic conductivity at room temperature can be improved by more than an order of magnitude when coinhibition of crystallite growth is promoted by the concerted behavior of the PEO:$LiClO_4$ and PEO:LiTFSI phases. Additionally, we examined the influence of mixed-salt ratio and total salt concentration on copolymer energetics, and we found that the slope of the effective interaction parameter (χ_{eff}) vs salt concentration in our lamellae-forming PS−PEO system was lower than that reported for a cylinder-forming PS−PEO system due to the balance between chain stretching and salt segregation in the PEO domains.

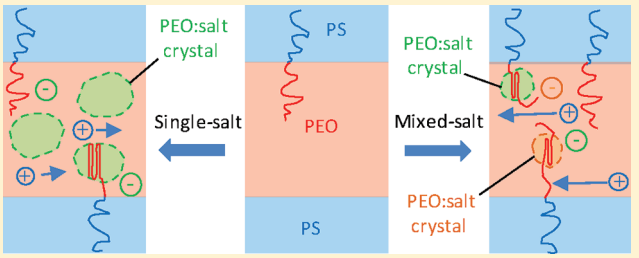

I. INTRODUCTION

Solid-state lithium batteries have attracted significant interest due to several desirable features including high energy density, good mechanical stability, and solvent free composition. A key component of these batteries is the electrolyte that facilitates ion transport between electrodes, and dry electrolyte systems with high mechanical strength are advantageous for avoiding thermal runaway reactions and dendrite formation during repeated charge−discharge cycles.[1] Block copolymers with well-defined ion-conducting pathways and a relatively high shear modulus have the potential to overcome the thermal and mechanical limitations of current electrolyte systems.[2,3] Poly(ethylene oxide)-based electrolyte systems have been the most popular for lithium batteries due to their promising ionic transport properties, which result from their high lithium salt solubilities and low glass transition temperatures.[4,5] However, because of the relatively low room temperature conductivities of these dry polymer electrolytes, lithium batteries containing PEO electrolytes are usually operated at elevated temperatures (typically >60 °C). In most cases, the low room temperature conductivity is caused by the crystallization of poly(ethylene oxide) (PEO) or PEO:salt complexes,[6] which reduce ionic conductivity by retarding segmental motion.[5]

Several methods have been proposed to extend the operating temperature range in non-block copolymer systems without using organic small-molecule plasticizers. Most approaches aim to decrease the melting temperature and the crystallinity of the polymer electrolyte. For example, in 1990, Armand et al. reported that it is possible to obtain a noncrystalline PEO electrolyte using a combination of $LiN(SO_2CF_3)_2$ (LiTFSI) salt and low molecular weight PEO (~4 kg/mol).[7−10] A crystallinity gap, between [EO]:[Li] = 12:1 and 6:1, was found in the PEO:LiTFSI phase diagram;[9] however, the crystallinity gap disappeared in higher molecular weight PEO systems.[11−13] Another approach by Craven et al. connected short chains of PEO with oxymethylene groups to produce a class of polymer that exhibited melting temperatures similar to their low molecular weight PEO analogues.[14] An additional avenue employed cross-linked PEO electrolytes to decrease the melting point and crystallinity, but the decreased chain mobility caused by cross-linking also led to a substantial reduction in ion conductivity.[15−17] Polymers with PEO side chains (i.e., comb-like copolymers) also exhibited successful suppression of PEO crystallization.[18] However, the length of the PEO side chain had to be optimized because the ionic conductivity was low if the side chain was too short,[19] and crystallization occurred if the side chain was too long.[20]

Instead of decreasing melting temperature or crystallinity, Bruce and co-workers found that some crystalline polymer electrolytes, $P(EO)_6$:$LiXF_6$ (X = P, As, or Sb), exhibited higher ionic conductivities than their amorphous analogues.[21] These crystalline polymer electrolytes provided stable conducting channels for ion transfer in their crystalline structure; furthermore, the ionic conductivity in these materials was improved by mixing different anions while maintaining the crystal structure.[22,23] However, the PEO molecular weight necessary to optimize the ionic conductivity for these

Received: June 10, 2011
Revised: August 19, 2011
Published: September 21, 2011

crystalline polymer electrolytes was very low, ~1 kg/mol. This low molecular weight enabled fast local segmental motion (which differs from the segmental motion in amorphous polymer electrolytes) and therefore increased ionic conductivity.[24] Unfortunately, the increase in mechanical strength afforded by using a crystalline polymer electrolyte or a cross-linking approach as mentioned above was not sufficient to prevent dendrite growth.

For block copolymer systems, most of the above-mentioned methods are not ideal for increasing ionic conductivity at room temperature. These methods either required low molecular weight PEO, which has been shown to give poor ionic conductivity in block copolymer systems,[2,3] or involved complicated synthesis procedures that are not easily adapted to lower cost block copolymers. Several reports used comb-like block copolymer systems, such as poly(methyl methacrylate-*b*-oligo-oxyethylene methacrylate) (PMMA−POEM),[25,26] poly(styrene-*b*-(ethylene glycol) methyl ether methacrylate-*b*-styrene) (PS−POEM−PS),[27,28] poly(styrene-*b*-(*p*-hydroxystyrene)-*g*-PEO)-*b*-styrene) (PS−P(S-*g*-EO)−PS),[29,30] and poly(styrene-*b*-(butadiene-*g*-ethylene oxide)-*b*-styrene) (PS−P(B-*g*-EO)−PS),[31,32] to achieve high room temperature ionic conductivities (>10^{-5} S/cm). However, the crystallization behavior in those salt-doped systems was not examined in detail. In contrast, PEO crystallization behavior in nondoped block copolymer systems has been reported. For example, in reports by Cheng and co-workers on a lamellae-forming poly(styrene-*b*-ethylene oxide) (PS−PEO) system, the PEO crystallite orientation and degree of crystallinity under nanoscale confinement by the PS domain were affected by the crystallization temperature.[33−35] In the context of block copolymer electrolytes, PS−PEO has been used as a model system because of the adequate mechanical strength and salt-solvating properties provided by the PS block and the PEO block, respectively.[2,3,36−40] Working within this framework, Balsara and co-workers found that the ionic conductivity of LiTFSI-doped PS−PEO increased as the PS−PEO molecular weight increased, and the maximum normalized ionic conductivity (σ_n) was 2/3 in the lamellae-forming PS−PEO system.[2,3] Also, using energy filtered transmission electron microscopy (EFTEM), they demonstrated increased segregation of the lithium salt to the middle of the PEO domain with increasing PS−PEO molecular weight.[37] In this work, we demonstrate a mixed-salt method, which can be easily used on current block copolymer electrolyte systems to increase their ionic conductivities at room temperature by decreasing the PEO/salt complex melting temperatures and degrees of crystallinity.

II. EXPERIMENTAL SECTION

Materials. The poly(styrene-*b*-ethylene oxide) (PS−PEO) diblock copolymer was synthesized via sequential anionic polymerization. First, the poly(styrene) (PS−OH) block was synthesized using *sec*-butyllithium as the initiator and then end-capped with ethylene oxide to generate a hydroxyl end group. Subsequently, the PS-OH was reinitiated with potassium naphthalenide to perform the ring-opening polymerization of ethylene oxide. The number-average molecular weight (M_n), polydispersity index (M_w/M_n), and PEO volume fraction (ϕ_{PEO}) of the synthesized PS−PEO were 25 600 g/mol, 1.04, and 0.49, respectively, as determined by gel permeation chromatography (Viscoteck 270max with Waters Styragel HR1 and HR4 columns) and ^{1}H nuclear magnetic resonance spectroscopy (Bruker AV-400) using homopolymer densities at 140 °C (ρ_{PS} = 0.969 g/mL, ρ_{PEO} = 1.064 g/mL).[41] Lithium perchlorate ($LiClO_4$) and LiTFSI were obtained from Aldrich and Alfa Aesar, respectively. The salts were dried under dynamic vacuum overnight before transfer into an argon-filled glovebox. PS−PEO and tetrahydrofuran (THF) also were dried rigorously before transfer into a glovebox due to the hygroscopic nature of the PEO:Li^+ complex. All further sample handling was performed in a glovebox or vacuum chamber. The salt-doped PS−PEO samples were prepared by mixing premeasured PS−PEO and salt(s) in dry THF, followed by solvent removal under dynamic vacuum. Samples are denoted as $SO_{x.x-y}$, where *x.x* represents the mixed-salt ratio ([LiTFSI]/([LiTFSI] + [$LiClO_4$]) = *x.x* = 0.0, 0.1, 0.5, 0.9, or 1.0) and *y* represents the salt-doping ratio ([EO]/[Li] = *y* = 12 or 6).

Small-Angle X-ray Scattering (SAXS). SAXS experiments were conducted in the Department of Chemical Engineering at the University of Delaware using a Rigaku SAXS instrument with 2 kW sealed-tube X-ray source (Cu Kα, λ = 1.54 Å) and a 2000 mm sample-to-detector distance. Sample temperature was controlled using a Linkam HFS91 CAP stage while acquiring scattering data under vacuum. SAXS sample cells were sealed in the glovebox before transferring into the vacuum chamber of the SAXS instrument. One-dimensional SAXS data are presented as azimuthally integrated logarithmic intensity vs the magnitude of the scattering vector, $q = |\mathbf{q}| = 4\pi\lambda^{-1}\sin(\theta/2)$, where θ is the scattering angle.

Transmission Electron Microscopy (TEM). A JEOL JEM-2000FX TEM was used to study the nanostructures of the polymer electrolyte samples. Thin sections (~70 nm thickness) of samples were obtained at −120 °C using a Leica Reichart Ultracut S microtome with a cryo-attachment. Samples were transferred and stored under a dry nitrogen environment until staining with ruthenium tetraoxide (RuO_4) at room temperature. The typical staining time was 90 s.

Differential Scanning Calorimetry (DSC). DSC experiments were conducted on a Mettler Toledo DSC 1 in the Center for Composite Materials at the University of Delaware. Samples were sealed in aluminum pans in the glovebox and stored in an argon environment prior to measurement. To study the effect of thermal history on crystallization, two sample preparation procedures were used. In the long crystallization procedure, the assembled sample pans were annealed in the antechamber of the glovebox at 150 °C under vacuum for 3 h, followed by crystallization in the glovebox refrigerator (0 ± 3 °C) for 3 months. Following crystallization, DSC experiments were conducted on these samples. The samples were cooled to 1 °C and held for 5 min and then heated up to 150 °C at 10 °C/min. The first heating curves are reported for these samples. In the short crystallization procedure, the assembled sample pans were annealed in the DSC at 150 °C for 0.5 h, cooled to 20 °C at 10 °C/min and held for 12 h, further cooled to 1 °C at 10 °C/min and held for 5 min, and then reheated to 150 °C at 10 °C/min. In this case, the second heating curves are reported.

Wide-Angle X-ray Scattering (WAXS). WAXS experiments were performed on the DND-CAT beamline (5-ID-D) at the Argonne National Laboratory (Advanced Photon Source). Two-dimensional scattering patterns were collected on a Roper Scientific CCD camera with an incident beam of wavelength λ = 0.7293 Å and a sample-to-detector distance of 158 mm. One-dimensional WAXS data are presented as azimuthally integrated logarithmic intensity vs the magnitude of the scattering vector, *q*.

AC Impedance Spectroscopy. The ionic conductivity was measured using a Princeton Applied Research PARSTAT 2273 frequency response analyzer with a homemade test cell on a Linkam HFS91 CAP stage. The samples were hot-pressed into disks under vacuum in the antechamber of a glovebox and then sandwiched between two blocking aluminum (Al) foil electrodes with a 0.5 mm thick Teflon O-ring as spacer. The contact area (*A*) between sample and Al foil was 0.32 cm^2 on each side. The impedance measurements were conducted under vacuum in either a standalone chamber or the sample chamber of the SAXS instrument. Samples were preannealed at 150 °C for 2 h to ensure good contact between the electrodes and the sample and then

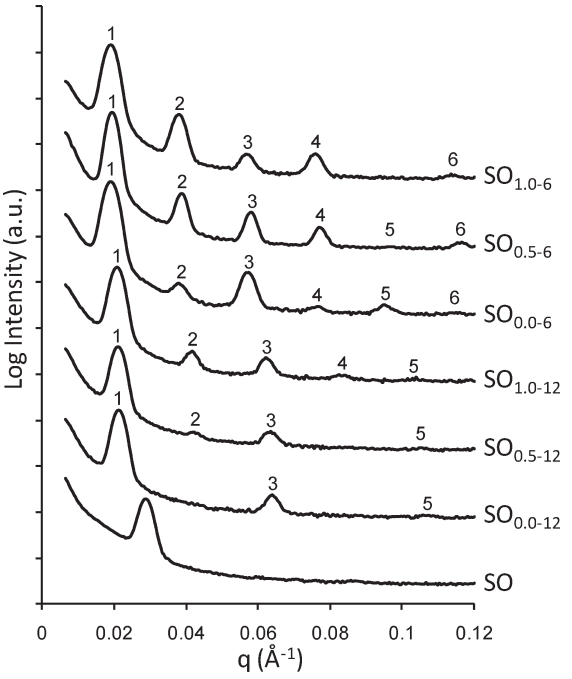

Figure 1. SAXS profiles of neat and salt-doped PS−PEO samples at various mixed-salt ratios and salt-doping ratios. The diffraction peaks are identified by q/q^*, where q^* is the primary diffraction peak. All of the salt-doped samples exhibited a lamellar morphology with Bragg reflection peaks located at q^*, $2q^*$, $3q^*$, $4q^*$, $5q^*$, and $6q^*$. The primary peak shifted to smaller q with increased salt loading (i.e., smaller [EO]:[Li] ratio), whereas the primary peak location exhibited negligible change with respect to the mixed-salt ratio. Curves were shifted vertically for clarity.

cooled to 20 °C at 30 °C/min and held for 12 h. The ionic conductivity was measured on heating between 20 and 150 °C. First and second impedance measurements were taken at each temperature with 5 and 8 min annealing times, respectively. We report the first measurement; the second measurement was used to ensure that stable ionic conductivity results were obtained during the process. The ac frequency range and voltage amplitude were 0.1−1 MHz and 10 mV, respectively. The bulk resistance of the electrolyte, R, was determined from the high-frequency plateau in the real impedance data, and the ionic conductivity, σ, was calculated using $\sigma = L/(RA)$, where L is the sample (Teflon O-ring) thickness.

III. RESULTS

The morphologies of neat and salt-doped PS−PEO samples were studied using a combination of SAXS and TEM. Typical SAXS profiles of neat and salt-doped PS−PEO samples at different mixed-salt and salt-doping ratios are shown in Figure 1. All SAXS data were acquired at 100 °C. The peaks are labeled as q/q^*, where q^* is the primary peak position. The scattering peaks of all salt-doped PS−PEO samples were consistent with a lamellar structure with Bragg reflection peaks located at q^*, $2q^*$, $3q^*$, $4q^*$, $5q^*$, and $6q^*$. The neat sample exhibited a diffraction peak at $q = 0.0287$ Å^{-1}, giving a domain spacing, d*, of 21.9 nm. The 12:1 salt-doping ratio samples all showed primary peaks between 0.0208 Å^{-1} ($SO_{1.0-12}$, $d^* = 30.2$ nm) and 0.0213 Å^{-1} ($SO_{0.0-12}$, $d^* = 29.5$ nm) whereas the 6:1 samples showed primary peaks between 0.0190 Å^{-1} ($SO_{1.0-6}$ and $SO_{0.0-6}$, $d^* = 33.1$ nm) and 0.0193 Å^{-1} ($SO_{0.5-6}$, $d^* = 32.6$ nm). As the salt concentration increased, the primary peaks shifted to smaller q values (larger domain spacings), but the mixed-salt ratio showed no significant

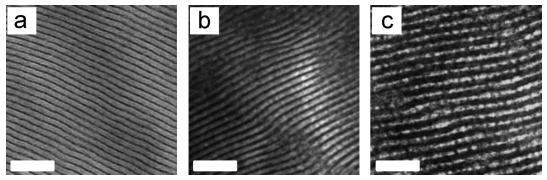

Figure 2. TEM images of SO (a), $SO_{0.0-12}$ (b), and $SO_{1.0-6}$ (c). Thin sections (~70 nm) of samples were obtained using a cryo-microtome at −120 °C under an N_2 atmosphere, and PEO domains were stained with RuO_4 vapor. The scale bars represent 100 nm.

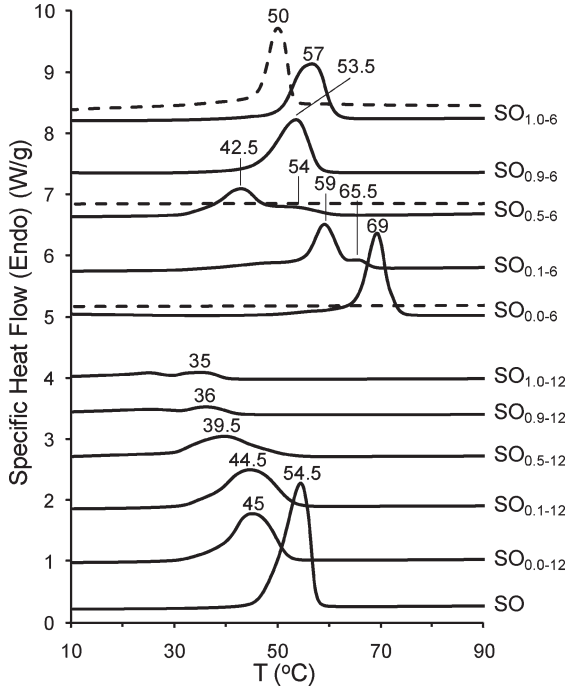

Figure 3. DSC traces of neat and salt-doped PS−PEO samples at various mixed-salt ratios and salt-doping ratios. The solid curves are the first heating curves of the samples after 3 months crystallization at 0 °C. The dashed curves are the second heating curves taken after 12 h crystallization at 20 °C. The heating rate was 10 °C/min for all samples.

effect on the primary peak position. The absence of the peak at $2q^*$ in $SO_{0.0-12}$ was likely the result of a minimum in the scattering form factor. The change in relative higher-order peak intensities at different mixed-salt ratios was also a result of changes in the scattering form factor with varying salt composition.

The TEM images shown in Figure 2 for SO (a), $SO_{0.0-12}$ (b), and $SO_{1.0-6}$ (c) also indicated a lamellar morphology for the neat and salt-doped samples. The domain spacings measured from the TEM images were 14.6, 16.2, and 23.3 nm for SO, $SO_{0.0-12}$, and $SO_{1.0-6}$, respectively. The domain spacing trend upon salt-doping measured from TEM was consistent with the SAXS data, and the deviation in values between SAXS and TEM was likely caused by sample shrinkage under exposure to the electron beam in the TEM. Also, the thickness of the darkened PEO domain increased as the salt concentration increased (volume fraction of PEO:salt complex increased). However, the fractions of the dark PEO domains in the images of SO and $SO_{0.0-12}$ were lower than 0.5 due to differences in staining rates for the samples at different salt concentrations.

dx.doi.org/10.1021/ma2013157 |*Macromolecules* 2011, 44, 8116–8123

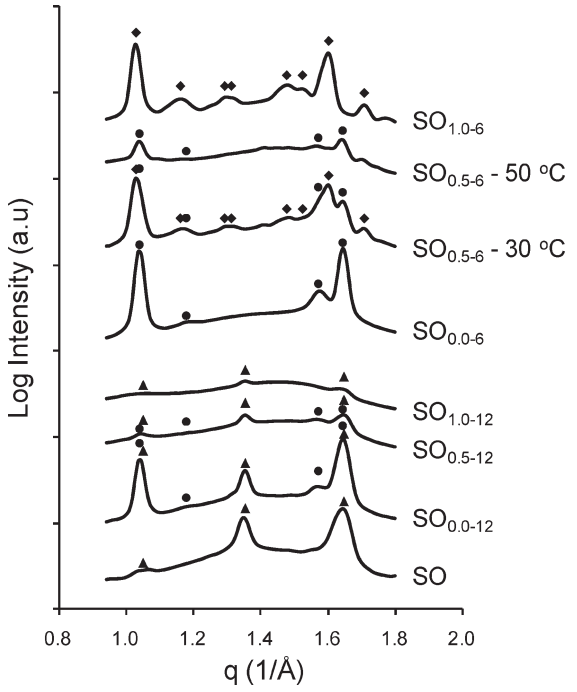

Figure 4. *In situ* WAXS profiles of neat and salt-doped PS−PEO samples. All data were obtained at 30 °C except for $SO_{0.5-6}$, which was acquired at 30 °C ($SO_{0.5-6}$ - 30 °C) and 50 °C ($SO_{0.5-6}$ - 50 °C). The triangles, circles, and diamonds on the curves mark the peak positions for the crystalline phases of PEO (▲),[6] $P(EO)_6$:$LiClO_4$ (●),[6] and $P(EO)_6$:LiTFSI (◆),[13] respectively.

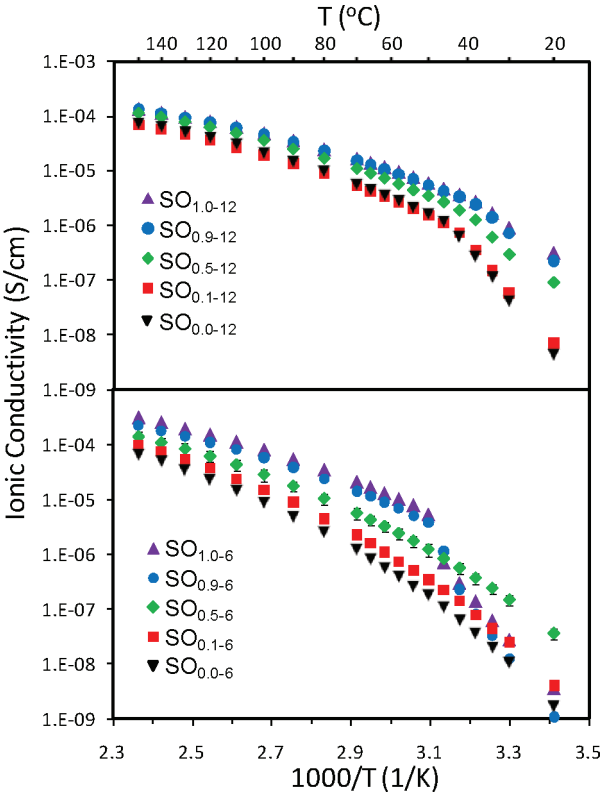

Figure 5. Ionic conductivity profiles of salt-doped PS−PEO samples at [EO]:[Li] = 12:1 (upper panel) and 6:1 (lower panel). Samples were annealed at 150 °C for 2 h and then cooled to 20 at 30 °C/min and held for 12 h before measurement on heating. The annealing time before each measurement was 5 min. The reported values are the average of multiple samples at each mixed-salt and salt-doping ratio, and the typical standard deviation is shown on the data for $SO_{0.5-6}$.

In Figure 3, we show the DSC traces for neat and salt-doped PS−PEO samples. Because of the slow crystallization of PEO:salt complexes, we prepared one set of samples via the long crystallization procedure (3 months at 0 °C) described in the Experimental Section to obtain melting temperatures (solid curves). The neat sample exhibited a melting peak at 54.5 °C, and integration of the peak area indicated that the PEO domain in the SO sample had 73.0% crystallinity (based on 196 J/g heat of fusion of PEO).[42] At the 12:1 salt-doping ratio, the melting point decreased gradually from 45 to 35 °C as the mixed-salt ratio increased from 0.0 (pure $LiClO_4$) to 1.0 (pure LiTFSI). The peak area also decreased as the mixed-salt ratio increased at the 12:1 salt-doping ratio. At the 6:1 salt-doping ratio, $SO_{0.0-6}$ (PS−PEO:$LiClO_4$) exhibited a melting peak at 69 °C. As the mixed-salt ratio increased, the melting point first decreased to 59 °C ($SO_{0.1-6}$), and 42.5 °C ($SO_{0.5-6}$) and then increased to 53.5 °C ($SO_{0.9-6}$) and 57 °C ($SO_{1.0-6}$). Both $SO_{0.1-6}$ and $SO_{0.5-6}$ had a high temperature shoulder adjacent to the main melting peaks. Using the mixed-salt ratio and the peak areas of $SO_{0.0-6}$ and $SO_{1.0-6}$, we estimated theoretical heats of fusion for mixed-salt specimens based on a linear interpolation between the $SO_{0.0-6}$ (PS−PEO:$LiClO_4$) and $SO_{1.0-6}$ (PS−PEO:LiTFSI) heats of fusion. (Note: we assumed that the $P(EO)_6$:$LiClO_4$ and $P(EO)_6$:LiTFSI complexes in the mixed-salt specimens had similar relative degrees of crystallinity to the pure salt specimens, i.e., $SO_{0.0-6}$ and $SO_{1.0-6}$, to calculate the interpolated theoretical values.) The heat of fusion of $SO_{0.5-6}$ obtained from DSC peak area was 72% of the interpolated theoretical value, while $SO_{0.1-6}$ and $SO_{0.9-6}$ were 87% and 98%, respectively. The second set of samples (dashed curves) was characterized following the short crystallization procedure (12 h at 20 °C) as described in the Experimental Section. After the short crystallization, $SO_{0.0-6}$ and $SO_{0.5-6}$ exhibited no melting peak above 0 °C, while $SO_{1.0-6}$ had a melting peak at 50 °C.

To determine the crystalline phases in each sample, WAXS experiments were performed at the DND-CAT (APS). Figure 4 shows the *in situ* WAXS profiles, acquired at 30 °C, for neat and salt-doped PS−PEO samples after the long crystallization process. Additional data were acquired at 50 °C for $SO_{0.5-6}$ ($SO_{0.5-6}$-50 °C) following the acquisition at 30 °C. The solid triangles, circles, and diamonds mark the expected reflection peak positions of PEO (▲),[6] $P(EO)_6$:$LiClO_4$ (●),[6] and $P(EO)_6$:LiTFSI (◆),[13] respectively. At [EO]:[Li] = 12:1, all samples exhibited reflection peaks similar to those noted for the SO specimen, corresponding to the PEO crystal structure. $SO_{0.0-12}$ and $SO_{0.5-12}$ also showed reflection peaks for $P(EO)_6$:$LiClO_4$ crystallites, but $SO_{1.0-12}$ did not show reflection peaks for $P(EO)_6$:LiTFSI crystallites. At [EO]:[Li] = 6:1, the $SO_{0.0-6}$ and $SO_{1.0-6}$ scattering data matched the expected peak characteristics for $P(EO)_6$:$LiClO_4$ and $P(EO)_6$:LiTFSI crystallites, respectively, and the $SO_{0.5-6}$ exhibited peaks from both 6:1 crystallites at 30 °C. After heating $SO_{0.5-6}$ to 50 °C, only two strong reflections at 1.04 and 1.64 $Å^{-1}$ remained. These peaks matched the two strong reflections from $P(EO)_6$:$LiClO_4$. On the basis of our long crystallization DSC results for $SO_{0.5-6}$, we expect that the crystallinity at 50 °C was related to the higher temperature shoulder for $SO_{0.5-6}$ in Figure 3. Thus, the combined WAXS and DSC data indicated that the main melting peak at 42.5 °C was from $P(EO)_6$:

dx.doi.org/10.1021/ma2013157 |*Macromolecules* 2011, 44, 8116–8123

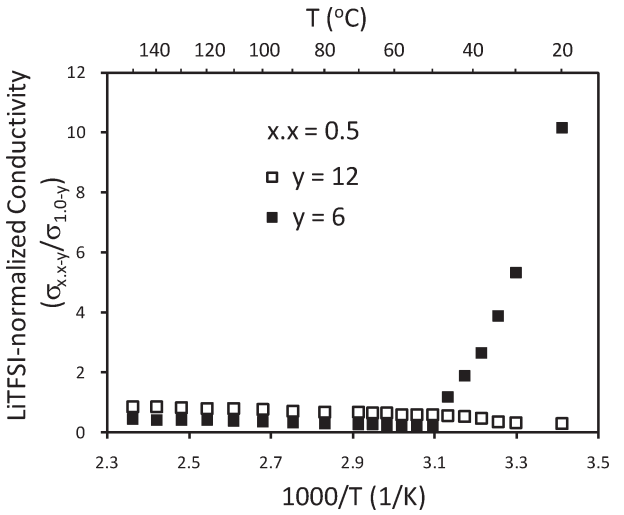

Figure 6. LiTFSI-normalized conductivity ($SO_{x.x-y}/SO_{1.0-y}$) profiles of $SO_{0.5-12}$ and $SO_{0.5-6}$ The open (□) and solid (■) squares represent the conductivity data for $SO_{0.5-12}$ and $SO_{0.5-6}$ normalized to the conductivity of $SO_{1.0-12}$ and $SO_{1.0-6}$, respectively, at each temperature.

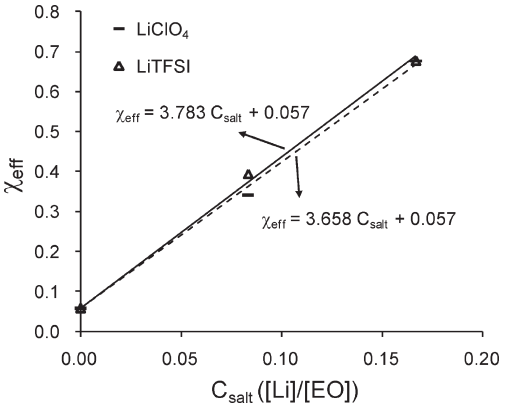

Figure 7. χ_{eff} vs C_{salt} ([Li]/[EO]) at 100 °C. The solid and dash lines are the least-squares fitting lines for LiTFSI-doped PS−PEO and $LiClO_4$-doped PS−PEO systems, respectively.

LiTFSI, and the higher temperature shoulder at 54 °C was from $P(EO)_6$:$LiClO_4$.

The ionic conductivity profiles of salt-doped PS−PEO samples are shown in Figure 5. The samples were preannealed at 150 °C for 2 h followed by 12 h crystallization at 20 °C before measurement on heating. (This protocol is similar to the DSC short crystallization procedure described above.) Data points shown in Figure 5 are the average values from two or three samples at each specific salt-doping ratio and mixed-salt ratio. The error bars on $SO_{0.5-6}$ are the standard deviation of the data acquired at 6:1 doping ratio and 0.5 mixed-salt ratio. Those error bars are representative of the error associated with all conductivity measurements. For the 12:1 doping ratio (upper panel), samples had nearly identical ionic conductivities at high temperatures. As the temperature decreased, the spread in ionic conductivities between samples at the various mixed-salt ratios increased. Additionally, the high-temperature conductivities of each sample changed gradually compared to their corresponding low-temperature counterparts. The steep trend in ionic conductivity at low temperature is due to contributions from the crystalline phase(s), in which the activation energy for ionic transport is high. The transition temperature between high- and low-temperature conductivity trends varied gradually from ≈46 °C ($SO_{0.0-12}$) to ≈38 °C ($SO_{1.0-12}$). Furthermore, we note that at 20 °C $SO_{0.1-12}$ exhibited a slightly higher ionic conductivity than $SO_{0.0-12}$, whereas $SO_{0.5-12}$ exhibited about an order of magnitude higher conductivity than $SO_{0.1-12}$.

At the 6:1 doping ratio (lower panel), $SO_{1.0-6}$ exhibited 5 times higher conductivity than $SO_{0.0-6}$ at 150 °C. For temperatures greater than 50 °C, the ionic conductivity of the 6:1 doping ratio samples increased as the mixed-salt ratio increased. For temperatures less than 50 °C, $SO_{0.9-6}$ and $SO_{1.0-6}$ exhibited sharp decreases in ionic conductivity compared to their higher temperature counterparts. The transition temperature of 50 °C for $SO_{1.0-6}$ matched the melting temperature as determined by DSC after 12 h crystallization at 20 °C. Though $SO_{0.9-6}$ and $SO_{1.0-6}$ exhibited transitions in conductivity behavior, $SO_{0.0-6}$, $SO_{0.1-6}$, and $SO_{0.5-6}$ showed no transitions at temperatures greater than 20 °C. This result is also consistent with the DSC results of $SO_{0.0-6}$ and $SO_{0.5-6}$ after 12 h crystallization at 20 °C, which showed no melting peaks at temperatures greater than 0 °C.

The LiTFSI-normalized conductivity ($SO_{x.x-y}/SO_{1.0-y}$) of $SO_{0.5-12}$ and $SO_{0.5-6}$ are shown in Figure 6. The LiTFSI-normalized conductivity of $SO_{0.5-12}$ (open squares) decreased slightly as the temperature decreased. However, the LiTFSI-normalized conductivity of $SO_{0.5-6}$ (solid squares) was greater than 1 at temperatures less than 46 °C and reached ~10 at 20 °C.

IV. DISCUSSION

The SAXS profiles and TEM images of neat and salt-doped PS−PEO samples revealed that the morphology of SO remained lamellar upon salt-doping to a 6:1 [EO]:[Li] doping ratio regardless of mixed-salt ratio. Thus, any effects of morphology on ionic conductivity were eliminated in this study.[43] The domain spacings calculated from SAXS profiles of neat and salt-doped samples varied from 21.9 nm (neat) to ≈30 nm ([EO]:[Li] = 12:1) and ≈33 nm ([EO]:[Li] = 6:1). The increase in domain spacing upon salt-doping was consistent with previous work on salt-doped cylinder-forming PS−PEO.[36,39,44−48] This domain size behavior is likely a result of chain conformations caused by PEO-salt association in the PS−PEO system. We estimated effective interaction parameters (χ_{eff}) vs salt-doping level and counterion composition using the domain spacing data for the $LiClO_4$-doped and LiTFSI-doped systems, where χ_{eff} was calculated from $d^* \sim \chi^{1/6}$, the relationship between domain spacing and χ for diblock copolymers in the strong segregation regime.[49,50] Details of this calculation can be found elsewhere.[39] The χ_{eff} of PS−PEO increased from 0.057 in the nondoped specimen to ≈0.370 at the 12:1 doping ratio and to ≈0.677 at the 6:1 doping ratio. Thus, we calculated a slope of χ_{eff} vs C_{salt} = 3.783 in the LiTFSI-doped PS−PEO system and a slope of 3.658 in the $LiClO_4$-doped PS−PEO system (where C_{salt} = [Li]/[EO]; see Figure 7). We note that this estimation did not take into account possible increases in segmental lengths and small deviations of the exponential dependence of d^* vs χ from 1/6.[51] Although these simplifications may cause a slight overestimation of χ_{eff}, the results still showed a reasonable relationship between salt-doping ratio and χ_{eff}. The slopes of the LiTFSI-doped system and the $LiClO_4$-doped system were nearly identical, supporting the hypothesis that the similar Lewis acidity of LiTFSI and $LiClO_4$ led to similar behavior when doped into PEO-containing

block copolymers.[39] We note that the slope of $LiClO_4$-doped PS−PEO in this study was lower than the slope obtained in a previous study on a cylinder-forming PS−PEO system, in which the slopes of χ_{eff} vs C_{salt} was 5.532 at 120 °C.[39] This lower slope can be explained by the free energy minimization of the system through chain stretching of the block copolymer and the nonuniform salt distribution in the PEO domain. As mentioned above, Balsara and co-workers found an increased nonuniform salt distribution in the PEO domains at higher segregation strengths.[37] This salt segregation behavior implies that a strong repulsion exists between the PS and the PEO:salt complex, and to minimize the system overall free energy, the PEO:salt complex separates from the PS domain. This repulsion behavior results in more chain stretching in a cylinder-forming PS−PEO than in a lamellae-forming PS−PEO at the same salt-doping ratio due to the geometry of the PEO domain. The greater chain stretching in the cylinder-forming system produces a larger increase in domain spacing, also indicating a larger increase in χ_{eff} for the cylinder-forming system compared to the lamellae-forming system at the same salt-doping level.

The DSC traces of salt-doped PS−PEO samples after the long crystallization process provided melting temperatures of the crystalline phases in each sample. Here, the crystallite size was not limited by the PEO domain thickness as the crystallite could grow along a direction perpendicular to the lamellar normal.[33] Although our long crystallization procedure was not optimized, the melting temperatures for $P(EO)_6$:$LiClO_4$ ($SO_{0.0-6}$) and $P(EO)_6$:LiTFSI ($SO_{1.0-6}$) were consistent with the values obtained by Robitaille and Fauteux in a PEO−$LiClO_4$ system and Lascaud et al. in a PEO−LiTFSI system.[6,9] Thus, the crystallite size was likely close to the maximum in our salt-doped PS−PEO samples after the long crystallization process. For the five mixed-salt ratios in this study, the melting temperatures in the 12:1 doping ratio system can be considered a weighted-average of the melting temperatures for the crystalline phases in $SO_{0.0-12}$ and $SO_{1.0-12}$. However, the trend for the 6:1 doping ratio system showed different behavior as the 0.5 mixed-salt ratio possessed the lowest melting temperature in the 6:1 doping ratio system. On the basis of estimated heat of fusion values, $SO_{0.5-6}$ exhibited roughly 72% of the crystallinity found in the $SO_{0.0-6}$ and $SO_{1.0-6}$ samples. Additionally, the *in situ* WAXS profiles for $SO_{0.5-6}$ indicated that the low temperature melting peak resulted from $P(EO)_6$:LiTFSI, and the high-temperature shoulder was from $P(EO)_6$:$LiClO_4$. Thus, the majority of the crystalline phases in $SO_{0.5-6}$ was $P(EO)_6$:LiTFSI. This result was reasonable as $P(EO)_6$:LiTFSI crystallization was favorable compared to $P(EO)_6$:$LiClO_4$ crystallization, as evidenced by the DSC traces of $SO_{0.0-6}$ and $SO_{1.0-6}$ after the short crystallization process (see Figure 3, dashed curves).

The conductivities of $LiClO_4$-doped samples ($SO_{0.0-12}$ and $SO_{0.0-6}$) and LiTFSI-doped samples ($SO_{1.0-12}$ and $SO_{1.0-6}$) shown in Figure 5 are relatively low compared to the numbers reported in the literature.[6,9] In fact, the conductivity values of $SO_{1.0-6}$ are only ≈6% of the corresponding conductivities of $P(EO)_6$:LiTFSI in the literature.[9] Considering that the volume fraction of the PEO was ≈0.5, the normalized conductivity of $SO_{1.0-6}$ was ≈0.18. ($\sigma_n = \sigma_{SO}/f/\varphi_{PEO}/\sigma_{PEO}$, where f is a morphology-related factor and is 2/3 for a lamellae case. σ_{SO} and σ_{PEO} are the ionic conductivities of the block copolymer electrolyte and the corresponding homopolymer electrolyte, respectively, at each temperature.) This value is consistent with the work by Balsara and co-workers[3] in which they found that the normalized conductivity increased as the molecular weight of block copolymer increased. Therefore, by increasing the PS−PEO molecular weight, the conductivity in our study should increase by a factor of 5 or more (up to $\sigma_n = 1$).

The ionic conductivity profiles of salt-doped PS−PEO samples with 12:1 salt-doping ratios all exhibited a transition between high- and low-temperature conductivity trends. This transition temperature moved from ≈46 to ≈38 °C as the mixed-salt ratio was varied from 0.0 to 1.0. This trend matched the melting point trend in the DSC results, which indicated that the mixed-salt approach did not decrease the melting temperature at the 12:1 doping ratio. From the WAXS profiles of $SO_{0.0-12}$ and $SO_{1.0-12}$ at 30 °C, we found that the majority crystalline phase in the 12:1 doping ratio samples was PEO, which may explain why the mixed salt failed to decrease the melting temperature and improve the room temperature ionic conductivity. The presence of a majority PEO crystalline phase implies that PEO crystallite growth is preferential to that of $P(EO)_6$:$LiClO_4$ and $P(EO)_6$:LiTFSI crystallites. Thus, replacing a certain amount of LiTFSI with $LiClO_4$ will not significantly alter the growth of crystallites that ultimately leads to a sharp reduction in ionic conductivity.

From the ionic conductivity profiles of the 6:1 doping ratio samples, transitions in conductivity behavior only occurred for $SO_{0.9-6}$ and $SO_{1.0-6}$. Comparison of the DSC traces of $SO_{0.0-6}$ and $SO_{1.0-6}$ after 12 h crystallization at 20 °C implied that crystallization was more favorable for $P(EO)_6$:LiTFSI than for $P(EO)_6$:$LiClO_4$. Therefore, in the 6:1 samples $P(EO)_6$:LiTFSI would crystallize first likely prohibiting the growth of $P(EO)_6$:$LiClO_4$ crystallites. However, $LiClO_4$-rich regions would also interrupt the growth of $P(EO)_6$:LiTFSI crystallites. As a result, the melting point and crystallinity decreased in $SO_{0.1-6}$, $SO_{0.5-6}$, and $SO_{0.9-6}$. Furthermore, the nucleation of $P(EO)_6$:LiTFSI was prohibited when enough $LiClO_4$ was present in the system as $P(EO)_6$:LiTFSI did not crystallize in $SO_{0.5-6}$ after the 12 h crystallization at 20 °C but did crystallize in $SO_{1.0-6}$ at the same temperature.

V. CONCLUSIONS

In this work we demonstrated a mixed-salt method to increase the room temperature ionic conductivities of block copolymer solid electrolytes. These electrolyte systems are especially suitable in solid-state lithium batteries, where a thermally, electrochemically, and mechanically stable electrolyte membrane with high ionic conductivity over a wide temperature range is needed. Using a mixed-salt system of $LiClO_4$ and LiTFSI, we found that the melting temperatures and degrees of crystallinity of the crystalline phases could be decreased in the PS−PEO system at [EO]:[Li] = 6:1. This reduction in melting temperature and crystallinity enabled us to obtain higher ionic conductivities at low temperatures compared to corresponding single-salt-doped PS−PEO electrolytes. We also found that the mixed-salt system showed no benefit on decreasing the melting point and crystallinity at [EO]:[Li] = 12:1 because the crystallization behavior in the 12:1 system was dominated by the PEO crystalline phase, which showed preferential crystallization compared to the $P(EO)_6$:$LiClO_4$ and $P(EO)_6$:LiTFSI phases and ultimately drove the decrease in ionic conductivity at this salt doping level. These results suggest that the use of a mixed-salt system can lead to a higher room temperature ionic conductivity in the appropriate block copolymer electrolyte system. Additionally, we examined the mixed-salt and salt concentration effects on block

copolymer energetics by estimating the χ_{eff} values in our lamellae-forming PS−PEO system using the domain spacing data from SAXS and the relationship between domain spacing and χ for block copolymers in the strong segregation regime. The LiTFSI-doped system and the $LiClO_4$-doped system showed similar slopes (χ_{eff} vs salt concentration), which were attributed to the close Lewis acidities of LiTFSI and $LiClO_4$ as previously postulated.[39]

AUTHOR INFORMATION

Corresponding Author
*E-mail: thepps@udel.edu.

ACKNOWLEDGMENT

We gratefully acknowledge AFOSR-PECASE (FA9550-09-1-0706) and ACS PRF Grant (PRF-46864-67) for financial support. J.N.L.A. was supported by the NSF through DMR-0645586 and a NSF Graduate Research Fellowship. The use of ^{1}H NMR instrumentation was supported by NSF CRIF: MU, CHE 0840401. We thank the W. M. Keck Electron Microscopy Facility for use of their TEM facilities. We also thank Steve Sauerbrunn (Mettler Toledo) and the Center for Composite Materials for use of their DSC instrument. Portions of this work were performed at the DuPont−Northwestern−Dow Collaborative Access Team (DND-CAT) located at Sector 5 of the Advanced Photon Source (APS). DND-CAT is supported by E.I. DuPont de Nemours & Co., The Dow Chemical Company, and the State of Illinois. Use of the APS facility was supported by the U.S. Department of Energy, Office of Science, Office of Basic Energy Sciences, under Contract DE-AC02-06CH11357.

REFERENCES

(1) Tarascon, J. M.; Armand, M. *Nature* **2001**, *414* (6861), 359–367.
(2) Singh, M.; Odusanya, O.; Wilmes, G. M.; Eitouni, H. B.; Gomez, E. D.; Patel, A. J.; Chen, V. L.; Park, M. J.; Fragouli, P.; Iatrou, H.; Hadjichristidis, N.; Cookson, D.; Balsara, N. P. *Macromolecules* **2007**, *40* (13), 4578–4585.
(3) Panday, A.; Mullin, S.; Gomez, E. D.; Wanakule, N.; Chen, V. L.; Hexemer, A.; Pople, J.; Balsara, N. P. *Macromolecules* **2009**, *42* (13), 4632–4637.
(4) Armand, M. B. *Annu. Rev. Mater. Sci.* **1986**, *16* (1), 245–261.
(5) Meyer, W. H. *Adv. Mater.* **1998**, *10* (6), 439–448.
(6) Robitaille, C. D.; Fauteux, D. *J. Electrochem. Soc.* **1986**, *133* (2), 315–325.
(7) Armand, M.; Gorecki, W.; Andreani, R. In *Second International Symposium on Polymer Electrolytes*; Scrosati, B., Ed.; Elsevier Applied Science: New York, 1990; pp 91−97.
(8) Vallee, A.; Besner, S.; Prud'Homme, J. *Electrochim. Acta* **1992**, *37* (9), 1579–1583.
(9) Lascaud, S.; Perrier, M.; Vallee, A.; Besner, S.; Prud'homme, J.; Armand, M. *Macromolecules* **1994**, *27* (25), 7469–7477.
(10) Gorecki, W.; Jeannin, M.; Belorizky, E.; Roux, C.; Armand, M. *J. Phys.: Condens. Matter* **1995**, *7* (34), 6823–6832.
(11) Edman, L.; Ferry, A.; Doeff, M. M. *J. Mater. Res.* **2000**, *15* (9), 1950–1954.
(12) Marzantowicz, M.; Dygas, J. R.; Krok, F.; Florjanczyk, Z.; Zygadlo-Monikowska, E. *J. Non-Cryst. Solids* **2006**, *352* (42−49), 5216–5223.
(13) Marzantowicz, M.; Dygas, J. R.; Krok, F.; Nowinski, J. L.; Tomaszewska, A.; Florjanczyk, Z.; Zygadlo-Monikowska, E. *J. Power Sources* **2006**, *159* (1), 420–430.
(14) Craven, J. R.; Mobbs, R. H.; Booth, C.; Giles, J. R. M. *Makromol. Chem., Rapid Commun.* **1986**, *7* (2), 81–84.
(15) Kono, M.; Furuta, K.; Mori, S.; Watanabe, M.; Ogata, N. *Polym. Adv. Technol.* **1993**, *4* (2−3), 85–91.
(16) Maccallum, J. R.; Smith, M. J.; Vincent, C. A. *Solid State Ionics* **1984**, *11* (4), 307–312.
(17) Rupp, B.; Schmuck, M.; Balducci, A.; Winter, M.; Kern, W. *Eur. Polym. J.* **2008**, *44* (9), 2986–2990.
(18) Ohno, H.; Inoue, Y.; Wang, P. *Solid State Ionics* **1993**, *62* (3−4), 257–264.
(19) Kobayashi, N.; Uchiyama, M.; Shigehara, K.; Tsuchida, E. *J. Phys. Chem.* **1985**, *89* (6), 987–991.
(20) Xia, D. W.; Soltz, D.; Smid, J. *Solid State Ionics* **1984**, *14* (3), 221–224.
(21) Stoeva, Z.; Martin-Litas, I.; Staunton, E.; Andreev, Y. G.; Bruce, P. G. *J. Am. Chem. Soc.* **2003**, *125* (15), 4619–4626.
(22) Christie, A. M.; Lilley, S. J.; Staunton, E.; Andreev, Y. G.; Bruce, P. G. *Nature* **2005**, *433* (7021), 50–53.
(23) Lilley, S. J.; Andreev, Y. G.; Bruce, P. G. *J. Am. Chem. Soc.* **2006**, *128* (37), 12036–12037.
(24) Bruce, P. G. *Dalton Trans.* **2006**, *11*, 1365–1369.
(25) Huang, B.; Cook, C. C.; Mui, S.; Soo, P. P.; Staelin, D. H.; Mayes, A. M.; Sadoway, D. R. *J. Power Sources* **2001**, *97−98*, 674–676.
(26) Ruzette, A.-V. G.; Soo, P. P.; Sadoway, D. R.; Mayes, A. M. *J. Electrochem. Soc.* **2001**, *148* (6), A537–A543.
(27) Nakano, H.; Dokko, K.; Sugaya, J.-i.; Yasukawa, T.; Matsue, T.; Kanamura, K. *Electrochem. Commun.* **2007**, *9* (8), 2013–2017.
(28) Niitani, T.; Shimada, M.; Kawamura, K.; Kanamura, K. *J. Power Sources* **2005**, *146* (1−2), 386–390.
(29) Hirahara, K.; Takano, A.; Yamamoto, M.; Kazama, T.; Isono, Y.; Fujimoto, T.; Watanabe, O. *React. Funct. Polym.* **1998**, *37* (1−3), 169–182.
(30) Se, K.; Miyawaki, K.; Hirahara, K.; Takano, A.; Fujimoto, T. *J. Polym. Sci., Part A: Polym. Chem.* **1998**, *36* (17), 3021–3034.
(31) Giles, J. R. M.; Gray, F. M.; MacCallum, J. R.; Vincent, C. A. *Polymer* **1987**, *28* (11), 1977–1981.
(32) Gray, F. M.; MacCallum, J. R.; Vincent, C. A.; Giles, J. R. M. *Macromolecules* **1988**, *21* (2), 392–397.
(33) Hsiao, M.-S.; Zheng, J. X.; Leng, S.; Van Horn, R. M.; Quirk, R. P.; Thomas, E. L.; Chen, H.-L.; Hsiao, B. S.; Rong, L.; Lotz, B.; Cheng, S. Z. D. *Macromolecules* **2008**, *41* (21), 8114–8123.
(34) Zhu, L.; Cheng, S. Z. D.; Calhoun, B. H.; Ge, Q.; Quirk, R. P.; Thomas, E. L.; Hsiao, B. S.; Yeh, F.; Lotz, B. *Polymer* **2001**, *42* (13), 5829–5839.
(35) Zhu, L.; Mimnaugh, B. R.; Ge, Q.; Quirk, R. P.; Cheng, S. Z. D.; Thomas, E. L.; Lotz, B.; Hsiao, B. S.; Yeh, F.; Liu, L. *Polymer* **2001**, *42* (21), 9121–9131.
(36) Young, W.-S.; Brigandi, P. J.; Epps, T. H. *Macromolecules* **2008**, *41* (17), 6276–6279.
(37) Gomez, E. D.; Panday, A.; Feng, E. H.; Chen, V.; Stone, G. M.; Minor, A. M.; Kisielowski, C.; Downing, K. H.; Borodin, O.; Smith, G. D.; Balsara, N. P. *Nano Lett.* **2009**, *9* (3), 1212–1216.
(38) Wanakule, N. S.; Panday, A.; Mullin, S. A.; Gann, E.; Hexemer, A.; Balsara, N. P. *Macromolecules* **2009**, *42* (15), 5642–5651.
(39) Young, W.-S.; Epps, T. H. *Macromolecules* **2009**, *42* (7), 2672–2678.
(40) Wanakule, N. S.; Virgili, J. M.; Teran, A. A.; Wang, Z.-G.; Balsara, N. P. *Macromolecules* **2010**, *43* (19), 8282–8289.
(41) Fetters, L. J.; Lohse, D. J.; Richter, D.; Witten, T. A.; Zirkel, A. *Macromolecules* **1994**, *27* (17), 4639–4647.
(42) Cheng, S. Z. D.; Wunderlich, B. *J. Polym. Sci., Part B: Polym. Phys.* **1986**, *24* (3), 577–594.
(43) Cho, B.-K.; Jain, A.; Gruner, S. M.; Wiesner, U. *Science* **2004**, *305* (5690), 1598–1601.
(44) Epps, T. H.; Bailey, T. S.; Pham, H. D.; Bates, F. S. *Chem. Mater.* **2002**, *14* (4), 1706–1714.
(45) Epps, T. H.; Bailey, T. S.; Waletzko, R.; Bates, F. S. *Macromolecules* **2003**, *36* (8), 2873–2881.
(46) Kim, S. H.; Misner, M. J.; Yang, L.; Gang, O.; Ocko, B. M.; Russell, T. P. *Macromolecules* **2006**, *39* (24), 8473–8479.

(47) Lee, D. H.; Kim, H. Y.; Kim, J. K.; Huh, J.; Ryu, D. Y. *Macromolecules* **2006**, *39* (6), 2027–2030.
(48) Lee, D. H.; Han, S. H.; Joo, W.; Kim, J. K.; Huh, J. *Macromolecules* **2008**, *41* (7), 2577–2583.
(49) Lipic, P. M.; Bates, F. S.; Matsen, M. W. *J. Polym. Sci., Part B: Polym. Phys.* **1999**, *37* (16), 2229–2238.
(50) Semenov, A. N. *Macromolecules* **1989**, *22* (6), 2849–2851.
(51) Whitmore, M. D.; Vavasour, J. D. *Acta Polym.* **1995**, *46* (5), 341–360.